MOX–Report No. 47/2011

Multigrid shape optimization governed by elliptic PDEs

Antonietti, P.F.; Borzì, A.; Verani, M.

MOX, Dipartimento di Matematica "F. Brioschi"
Politecnico di Milano, Via Bonardi 9 - 20133 Milano (Italy)

mox@mate.polimi.it http://mox.polimi.it

Multigrid shape optimization governed by elliptic PDEs

Paola F. Antonietti[♮], Alfio Borzì[♭], Marco Verani[♮]

December 23, 2011

[♮] MOX, Dipartimento di Matematica, Politecnico di Milano,
Piazza Leonardo da Vinci 32, 20133 Milano, Italy
paola.antonietti@polimi.it, marco.verani@polimi.it

[♭] Institut für Mathematik, Universität Würzburg,
Campus Hubland Nord, Emil-Fischer-Str. 30, 97074 Würzburg, Germany.
alfio.borzi@mathematik.uni-wuerzburg.de

Abstract

This paper presents and analyzes a new multigrid framework to solve shape optimization problems governed by elliptic PDEs. The boundary of the domain, i.e., the control variable, is represented as the graph of a continuous function that is approximated at various levels of discretization. The proposed multigrid shape optimization scheme acts directly on the function describing the geometry of the domain and it combines a single-grid shape gradient optimizer with a coarse-grid correction (minimization) step, recursively within a hierarchy of levels. The convergence of the proposed multigrid shape optimization method is proved and several numerical experiments assess its effectiveness.

1 Introduction

Starting with the foundation of PDE-based optimization [21], shape design has been one of the most frequent application in technologies and it is nowadays one main focus of aerodynamics simulation. A central role in the formulation and development of computational frameworks for shape optimization has been played by elliptic shape optimization problems [26] that correspond to cases of potential flow allowing simpler investigation. Nevertheless, these problems arise in many important applications as nozzle and airfoil design [26, 33], and in the design of beams and plates [28]. Along this development, one of the most remarkable advances in shape design has been to replace the approach of parametric optimization with the concept of continuous shape design. In fact, in the former approach the control variable (i.e., the shape) is restricted to belong to a finite dimensional space spanned by suitable basis functions, while in the latter case it is an element of an infinite-dimensional space. This second approach opens enormous perspective in the formulation of more accurate and sophisticated shape optimization problems.

The possibility of formulating the shape optimization problems at the infinite-dimensional level poses new challenges to the design and implementation of numerical optimization schemes that properly accommodate the infinite dimensionality of the control function. In particular, a successful and effective algorithm must allow the control function to be approximated and optimized to any desired degree of accuracy. On the other hand, we notice that the shape optimization problems under consideration are governed by partial differential equations where the issue of solving up to a desired accuracy also arises. It is therefore reasonable to consider a unique approximation framework for the PDE solution and for the shape optimal design. This is readably possible with most discretization methods for PDEs (e.g. based on finite elements, finite volumes or mimetic finite differences) by considering the underlying decomposition as an approximation of the optimal shape. This point of view suggests that it could be advantageous to design efficient optimization schemes based on principles that are successful in the formulation of fast PDE solvers [3]. The purpose of this paper is to formulate and analyze a multigrid shape optimization framework that extends principles and techniques of the multigrid strategy for PDE solvers and accommodates the infinite-dimensionality of the control variables. We notice that an alternative approach to the framework presented in this paper is to include the geometric informations into the coefficients of the governing equations and to apply to them the standard multigrid method. However, the novelty and the challenge of this work is to present a multigrid framework that acts directly on the geometric variable.

In shape optimization processes a convenient approach to manage shape changes is to model the control boundary as the graph of a continuous function [4, 26, 17, 19]. We observe that the resulting class of admissible configurations is typically satisfactory for most of industrial applications. This approach is common in the method of mapping where the physical domain is mapped onto a computational domain that is easier to describe. On the other hand, modeling the boundary as the graph of a function results very convenient to enforce the desired regularity to the domain and to include additional geometrical constraints.

For these reasons, our multigrid shape optimization (MGSO) scheme hinges upon the definition of the optimization boundary as a regular function that is discretized together with the domain by a hierarchy of finite-element grids. Our approach is in contrast to previous attempts [6, 9, 10, 11, 12, 8] to define a consistent multigrid framework for shape optimization where the computational domain is discretized by finite elements and the control boundary is represented through parameterized shape functions. Therefore, within the hierarchy of levels defined by the multigrid strategy, our approach makes possible to construct a coarse-grid correction step that can be understood from the geometrical [31] and optimization [2, 3, 20, 24, 32] point of views, whereas the idea in [6, 9] of coarsening by taking a subset of shape parameters appears based on heuristic consideration.

As we focus on multigrid concepts, we need to define an iterative optimization process that can be applied at any level of discretization with the aim of improving the shape towards the optimum. In our case, this is a shape-gradient optimizer that acts similarly to a Jacobi smoother in a classical multigrid scheme. For this purpose, we need to evaluate the shape gradient at any point of the triangulation: this is possible using the Hadamard representation of the shape gradient [28]. We also choose to derive the shape gradient expression in the Hadamard form because it enables a very efficient computation of the gradient without the need of computing

the so called "mesh sensitivity" Jacobian. This is especially important for aerodynamic quantities such as drag and lift coefficients and for matching a target surface pressure distribution. Moreover, the Hadamard approach provides a continuous representation of the gradient function that is required in a multigrid framework. Indeed, as the mesh is refined the gradient function is required at increasingly many points of the boundary. We notice that this framework is valid in any spatial dimension and can be also extended to deal with adaptive mesh refinement strategies for shape optimization [23].

In addition to the iterative scheme mentioned above, the formulation of a multigrid scheme requires to define a coarse-grid correction step that complements the action of the single-grid optimization procedure. To construct this step, suitable intergrid transfer operators are required together with the formulation of a coarse optimization problem that appropriately approximates the fine-level shape optimization problem. In our approach, we exploit the fact that the optimization function is the graph of a sufficiently regular function and choose the intergrid transfer operators as in the case of classical multigrid schemes defined on manifolds [18, 1], i.e., as geometric interpolation and restriction operators. On the other hand, to define the coarse shape optimization problem, we extend the multigrid optimization framework introduced in [20, 24] to the present case where the optimization variable is a geometrical object.

Our multigrid shape optimization strategy appears very appealing since it allows to prove convergence of the resulting algorithm to a local optimal solution by requiring typical differentiability properties and local positiveness of the reduced shape Hessian. For the purpose of this analysis, we extend the theoretical framework introduced in [2, 32].

The outline of the paper is as follows. In Section 2, we introduce our framework that identifies the geometric control variable with a continuous function belonging to a Hilbert space. Based on this formulation, we illustrate the concepts of shape derivative and shape gradient, and focus on a representative elliptic PDE shape optimization problem with the goal of minimizing a volume cost functional complemented with suitable (area and perimeter) penalization terms. For this problem, we compute the shape gradient and correspondingly define a globalized gradient-based shape optimization procedure. In Section 3, we formulate the multigrid shape optimization scheme based on a hierarchy of shape optimization problems. We define the intergrid transfer operators and illustrate the construction of the coarse-grid shape optimization problem. We also investigate the optimization properties of the multigrid components and prove that the coarse-grid correction provides a minimizing step. In Section 4, we numerically validate our multigrid shape optimization scheme considering different test problems. In particular, we investigate the robustness of the multigrid scheme with respect to the choice of the initial shape profile and of the granularity of the mesh. A section of conclusion completes the exposition of this work.

2 The Shape Optimization problem

Consider the class of domains

$$\Omega = \{(x,y) \in \mathbb{R}^2 : \quad x \in I = (a,b) \text{ and } y \in (\varphi(x), \psi(x) + u(x))\} \tag{1}$$

where $\varphi(x), \psi(x)$ and $u(x)$ are given functions with $\varphi(x) < \min(\psi(x), \psi(x) + u(x))$ and $(x, \psi(x))$, $x \in I$, represents the segment with end points $\mathbf{A} = (a, \psi(a))$ and $\mathbf{B} = (b, \psi(b))$. In the following, for simplicity we choose $\varphi(x) = -M$ and $\psi(x) = 0$.

The deformable boundary of Ω is denoted by Γ and it is parametrized by a function $u \in \mathcal{U}_{ad}$ (see Figure 0(a)), with

$$\mathcal{U}_{ad} = \{u \in C^{0,1}(I) : -M < \beta_1 \leq u(x) \leq \beta_2 \text{ and } u(a) = u(b) = 0\} . \tag{2}$$

Hence, in the following shape optimization problem the boundary

$$\Gamma = \{(x, u(x)) \in \mathbb{R}^2 : \quad \forall x \in I \text{ and } u \in \mathcal{U}_{ad}\} \tag{3}$$

is the geometric control variable while $\Gamma^F = \partial\Omega \setminus \bar{\Gamma}$ is fixed.

The extension to the more general 2D situation depicted in Fig 0(b) or to analogous 3D configurations is straightforward, but for the ease of reading it will not be further considered.

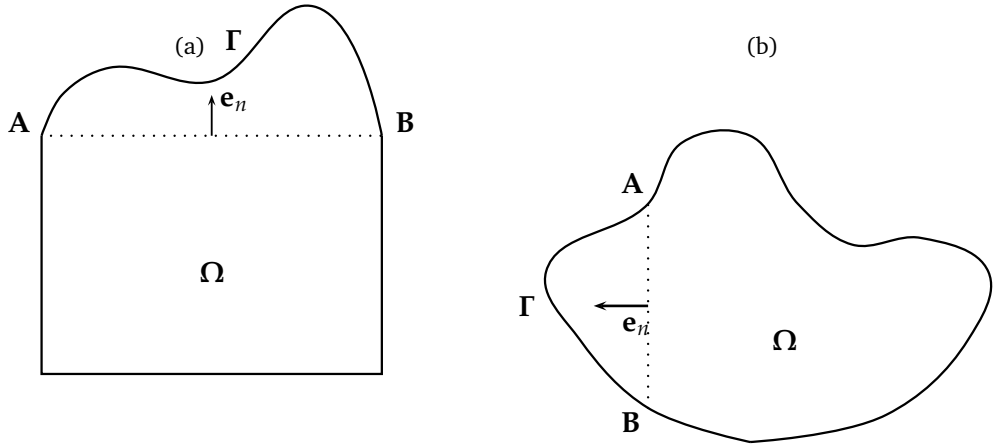

Figure 1: The control boundary Γ as a function.

We now introduce our shape optimization problem. Let $y = y(\Omega)$ be the unique solution to the following elliptic partial differential equation

$$\begin{aligned} -\Delta y &= f \qquad \text{in } \Omega & (4)\\ y &= y_b \qquad \text{on } \partial\Omega\,, & (5) \end{aligned}$$

where y_b is a given function defined in $\mathbb{R}^2$. Let r be a given function and $\lambda_1, \lambda_2, A, P > 0$ be given positive parameters. We consider the following cost functional

$$J(y, \Omega) := \int_\Omega r(y)\, d\Omega + \frac{\lambda_1}{2}\left(\int_{\partial\Omega} d\Gamma - P\right)^2 + \frac{\lambda_2}{2}\left(\int_\Omega d\Omega - A\right)^2, \tag{6}$$

which depends on the solution y of the problem (4)-(5), on the difference between the perimeter of $\partial\Omega$ and a given target value P and on the difference between the area of Ω and a given target value A. In the following, we will denote by $|\Omega|$ and $|\partial\Omega|$ the area and the perimeter of Ω, respectively.

It is clear that a perturbation of Γ corresponds to a perturbation of Ω which results in a variation of the solution of the boundary value problem and hence of the cost functional. Therefore, we can consider the following mapping

$$\Gamma \to y(\Omega) \tag{7}$$

that we assume to be Fréchet differentiable. Using the mapping (7), we can define the following reduced objective functional

$$\hat{J}(\Gamma) = J(y(\Omega), \Omega). \tag{8}$$

We are interested in solving the following shape optimization problem

$$\Gamma^* = \text{argmin}_{\Gamma \in \mathcal{U}_{ad}} \hat{J}(\Gamma) \ ,$$

where by abuse of notation we identify $\mathcal{U}_{ad}$ with the set of admissible boundaries.

In order to define the gradient of $\hat{J}(\Gamma)$ with respect to a variation of Γ, we introduce a family of mappings $T_t : x \mapsto T_t(x)$ given by the perturbation of the identity

$$T_t(x) = x + t\, V(x),$$

where $V \in \mathbb{R}^2$ is a vector field of appropriate smoothness. Under this mapping, a deformed domain Ω_t is given by

$$\Omega_t := \{T_t(x) : \ x \in \Omega\}$$

with boundary $\Gamma_t = \{T_t(x) : x \in \Gamma\}$. If y_t denotes the solution of the constraint equation (4)-(5) in the perturbed domain Ω_t, we seek to derive a formula for the shape derivative

$$d\hat{J}(\Gamma)[V] := \lim_{t \to 0^+} \frac{\hat{J}(\Gamma_t) - \hat{J}(\Gamma)}{t} \ .$$

Using the so-called Hadamard representation formula (see e.g. [28]) , the shape derivative $d\hat{J}$ reads as follows

$$d\hat{J}(\Gamma)[V] = \int_\Gamma \nabla \hat{J}(\Gamma)\, \mathrm{v}\, dS,$$

where $\nabla \hat{J}(\Gamma)$ is the reduced shape gradient and $\mathrm{v} = \langle V, \nu \rangle$ is the normal component of the vector field V. It is easy to prove (see e.g. [28]) that the shape derivative for the elliptic problem (4)-(5) is

$$d\hat{J}(\Gamma)[V] := \int_\Gamma \left(r(y) - \frac{\partial p}{\partial \nu} \frac{\partial (y_b - y)}{\partial \nu} \right) \mathrm{v}\, dS + \lambda_1 \left(|\partial\Omega| - P \right) \int_\Gamma K\mathrm{v}\, dS + \lambda_2 \left(|\Omega| - A \right) \int_\Gamma \mathrm{v}\, dS$$

where K is the mean curvature of Γ, y is the solution to (4)-(5) and p is the solution to the following adjoint problem

$$\begin{aligned} -\Delta p &= \frac{\partial r(y)}{\partial y} \qquad \text{in } \Omega \\ p &= 0 \qquad \text{on } \partial\Omega. \end{aligned}$$

As an example, for homogeneous $y_b = 0$ we have $\frac{\partial y_b}{\partial \nu} = 0$ on $\partial\Omega$.

Based on the reduced gradient, we can define a preconditioned gradient-based shape optimization (GSO) scheme (see e.g. [7, 13, 15]) that constructs a sequence of optimization boundaries $\{\Gamma^\ell\}_{\ell\in\mathbb{N}}$ through the following update

$$\Gamma^{\ell+1} = \{x + t_\ell \, \mathbb{S}(\nabla \hat{J}(\Gamma^\ell)) \, \mathbf{e}_n, \, x \in \Gamma^\ell\},$$

where $\mathbf{e}_n$ denotes the unit vector oriented as the perpendicular to the segment $\overline{\mathbf{AB}}$ in the domain's outwards direction (see Figure 1), $\mathbb{S}$ is a suitable preconditioner (e.g., $\mathbb{S} = -{\Delta_\Gamma}^{-1}$, being Δ_Γ the Laplace-Beltrami operator) and t_ℓ is a steplength obtained by linesearch [25], such that

$$\hat{J}(\Gamma^{\ell+1}) < \hat{J}(\Gamma^\ell).$$

The GSO algorithm reads as follows

Algorithm 2.1 (Gradient-based shape optimization (GSO) scheme - m-steps)**.** *Let Γ^0 be the starting optimization boundary, set the index $\ell = 0$. We have the following intermediate steps.*

Step 1. Solve the forward problem

$$\begin{aligned} -\Delta y^\ell &= f \qquad \text{in } \Omega^\ell \\ y^\ell &= y_b \qquad \text{on } \partial\Omega^\ell. \end{aligned}$$

Step 2. Solve the adjoint problem

$$\begin{aligned} -\Delta p^\ell &= \frac{\partial r(y^\ell)}{\partial y} \qquad \text{in } \Omega^\ell \\ p^\ell &= 0 \qquad \text{on } \partial\Omega^\ell. \end{aligned}$$

Step 3. Setup the gradient

$$\nabla \hat{J}(\Gamma^\ell)(x) = \left(r(y^\ell) - \frac{\partial p^\ell}{\partial \nu} \frac{\partial (y_b - y^\ell)}{\partial \nu} + \lambda_1 \left(|\partial\Omega^\ell| - P \right) K \right. \\ \left. + \lambda_2 \left(|\Omega^\ell| - A \right) \right)(x), \quad x \in \Gamma^\ell.$$

Step 4. Update the boundary using linesearch

$$\Gamma^{\ell+1} = \{x + t_\ell \, \mathbb{S}(\nabla \hat{J}(\Gamma^\ell)) \, \mathbf{e}_n, \, x \in \Gamma^\ell\} \, .$$

Step 5. If $\ell < m$, increment index $\ell = \ell + 1$ and goto Step 1.

In the following, one step of the GSO scheme defined by Algorithm 2.1 is denoted with $\Gamma^{\ell+1} = G(\Gamma^\ell)$.

3 The multigrid shape optimization framework

This is the main section of the paper where we illustrate the elements of our multigrid shape optimization framework. In particular, in Section 3.1 we introduce the hierarchy of discrete control boundaries, while in Section 3.2 we define the inter-grid transfer operators acting between the different levels of this hierarchy. Finally, in Section 3.3 we discuss the formulation and the properties of the key ingredients of our multigrid shape optimization scheme, namely the coarse-grid shape optimization problem and the resulting coarse-grid correction step. At the end of Section 3.3 the complete algorithm is reported.

3.1 The discrete setting

We first introduce the hierarchy of discrete control boundaries. Let $\mathcal{T}_k(I)$ be a triangulation of the interval I. Let $k \in \mathbb{N}^+$ denote the level of discretization and $h_k = \frac{b-a}{N_k}$ (e.g., $N_k = 2^{k+1}$) the associated mesh-size. We set $x_j = a + jh_k$ with $j = 0, \ldots, N_k$ and we denote by $I_j = [\, x_{j-1}, x_j \,]$ the j-th element of $\mathcal{T}_k(I)$. The space of *discrete* admissible configurations is defined as follows

$$\mathcal{U}_{ad}^k = \{u_k \in \mathcal{U}_{ad} : \quad u_k|_{I_j} \in \mathbb{P}^1(I_j) \text{ for } j = 1, \ldots, N_k\} \subset \mathcal{U}_{ad} \,,$$

where $\mathbb{P}^1(I_j)$ is the space of univariate polynomials on I_j with degree less than or equal to one. According to this, Ω_k will denote the domain parametrized by u_k and Γ_k the corresponding piecewise linear mobile boundary (see Figure 1(a)).

(a) Triangulations at k-th level of discretization: $I_j \in \mathcal{T}_k(I)$, $\hat{I}_j \in \mathcal{T}_k(\Gamma_k)$

(b) The discrete control boundary at different levels of discretization: Γ_k (dotted) and $\Gamma_{k-1} = I_k^{k-1}\Gamma_k$ (solid).

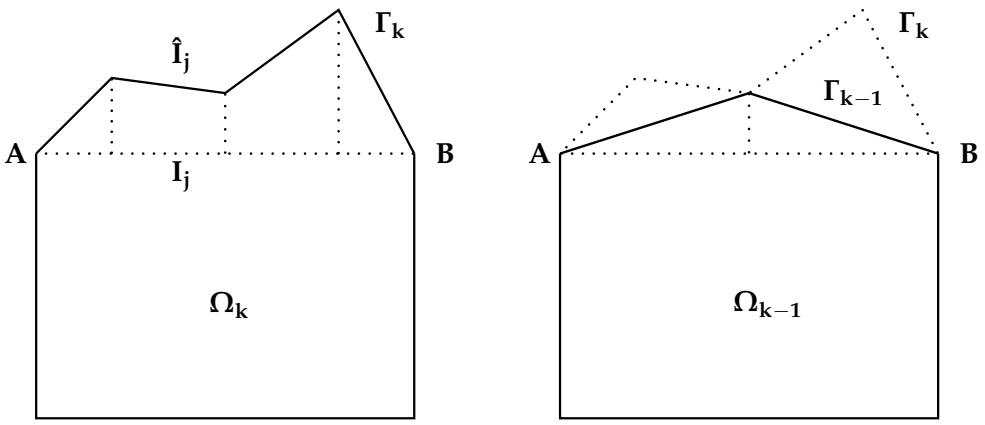

Figure 2: The discrete setting at different levels of discretization.

Let us now introduce the finite element space to approximate the solution of the PDE on Ω_k. Let $\mathcal{T}_k(\Omega_k)$ be a conforming and shape-regular triangulation of Ω_k, where we assume that every node $\hat{x}_j := u(x_j)$ is a vertex of $\mathcal{T}_k(\Omega_k)$. We denote by

h_k be the diameter of an element $T \in \mathcal{T}_k(\Omega_k)$. Let $\mathbb{V}(\Omega_k)$ be the space of linear finite elements

$$\mathbb{V}(\Omega_k) = \{v \in H_0^1(\Omega_k) \ : \ v|_T \in \mathbb{P}^1(T) \ \forall T \in \mathcal{T}_k(\Omega_k)\},$$

where $\mathbb{P}^1(T)$ represents the space of polynomial functions on T of degree less or equal than 1. Let us assume $y_b \in \mathbb{V}(\Omega_k)$, we denote by $y_k \in \mathbb{V}(\Omega_k) \oplus y_b$ the finite element approximation to the exact solution y of (4)-(5). Finally, if we define the discrete reduced functional $\hat{J}_k(\Gamma_k)$ at k-level as

$$\hat{J}_k(\Gamma_k) := J(y_k(\Omega_k), \Omega_k) \tag{9}$$

then the reduced discrete shape optimization problem at level k reads as follows:

$$\Gamma_k^* = \text{argmin}_{\Gamma_k \in \mathcal{U}_{ad}^k} \hat{J}_k(\Gamma_k) \ . \tag{10}$$

3.2 Intergrid transfer operators

For multigrid purpose, we need to define intergrid transfer operators acting on

- functions in $\mathcal{U}_{ad}^k$;
- geometric boundaries Γ_k;
- functions defined on geometric boundaries (i.e., shape gradients).

We first deal with functions in $\mathcal{U}_{ad}^k$. In the spirit of [18], we define a restriction operator $I_k^{k-1} : \mathcal{U}_{ad}^k \to \mathcal{U}_{ad}^{k-1}$ acting as sketched in Figure 1(b). The corresponding prolongation operator $I_{k-1}^k : \mathcal{U}_{ad}^{k-1} \to \mathcal{U}_{ad}^k$ is defined so that the following relation holds

$$(I_k^{k-1}u, v)_{L^2(I)} = (u, I_{k-1}^k v)_{L^2(I)} \tag{11}$$

for all $u \in \mathcal{U}_{ad}^k$ and $v \in \mathcal{U}_{ad}^{k-1}$. Accordingly, we can define a *geometric* restriction operator and a corresponding geometric prolongation operator. Let Γ_k be the mobile part of the domain Ω_k parametrized by $u_k \in \mathcal{U}_{ad}^k$, we define by Γ_{k-1} the boundary parametrized by $u_{k-1} = I_k^{k-1}u_k$. By abuse of notation, we write

$$\Gamma_{k-1} = I_k^{k-1}\Gamma_k \qquad \Gamma_k = I_{k-1}^k \Gamma_{k-1} \ .$$

We now introduce a pair of transfer operators acting on the functions defined on discrete boundaries; this will be useful to restrict/prolongate shape gradients from Γ_k to Γ_{k-1} and viceversa. We build a triangulation $\mathcal{T}_k(\Gamma_k)$ of Γ_k as follows: the function u_k (which parametrizes Γ_k) induces a one-to-one correspondence between elements $I_j \in \mathcal{T}_k(I)$ and elements $\hat{I}_j \in \mathcal{T}_k(\Gamma_k)$ which results to be defined by

$$\hat{I}_j = \{(x, u_k(x)) : \quad x \in I_j\}$$

(see Figure 1(a)). Let $\mathbb{V}(\Gamma_k)$ be the space of piecewise linear functions defined on $\mathcal{T}_k(\Gamma_k)$. We define a *functional* restriction operator $\mathcal{I}_k^{k-1} : \mathbb{V}(\Gamma_k) \to \mathbb{V}(\Gamma_{k-1})$ and a corresponding functional prolongation operator $\mathcal{I}_{k-1}^k : \mathbb{V}(\Gamma_{k-1}) \to \mathbb{V}(\Gamma_k)$. We require that they satisfy the following

$$(\mathcal{I}_k^{k-1}g, h)_{\Gamma_{k-1}} = (g, \mathcal{I}_{k-1}^k h)_{\Gamma_k} \tag{12}$$

for all $g \in \mathbb{V}(\Gamma_k)$ and $h \in \mathbb{V}(\Gamma_{k-1})$, where $(\cdot,\cdot)_{\Gamma_k}$ denotes the inner product in $\mathbb{V}(\Gamma_k)$ to be defined later. Let $g \in \mathbb{V}(\Gamma_k)$, the functional restriction operator is defined as follows

$$\mathcal{I}_k^{k-1} g = \left[I_k^{k-1}(\, g^{\#}{}_{|I} \,) \right]^{\#}_{|\Gamma_{k-1}} , \tag{13}$$

where $g^{\#}$ is the extension of g to $I \times \mathbb{R}$ defined as

$$g^{\#}(x,y) = g(u_k(x)) \quad \forall x \in I, \, \forall y \in \mathbb{R} , \tag{14}$$

being u_k the parametrization of Γ_k. The functional prolongation operator $\mathcal{I}_{k-1}^k$ can be defined in an analogous way. By introducing the inner product in $\mathbb{V}(\Gamma_k)$ as

$$(f,g)_{\Gamma_k} := (\, f^{\#}{}_{|I} \, , \, g^{\#}{}_{|I} \,)_{L^2(I)} \qquad \text{for all } f,g \in \mathbb{V}(\Gamma_k) , \tag{15}$$

it is easy to verify the validity of (12). Indeed, there holds

$$\begin{aligned} (g, \mathcal{I}_{k-1}^k h)_{\Gamma_k} &= (\, g^{\#}{}_{|I} \, , \, [\mathcal{I}_{k-1}^k h]^{\#}{}_{|I} \,)_{L^2(I)} \\ &= (\, g^{\#}{}_{|I} \, , \, I_{k-1}^k (h^{\#}{}_{|I}) \,)_{L^2(I)} \\ &= (\, I_k^{k-1}(g^{\#}{}_{|I}) \, , \, h^{\#}{}_{|I} \,)_{L^2(I)} \\ &= (\, \mathcal{I}_k^{k-1} g \, , \, h \,)_{\Gamma_{k-1}} , \end{aligned}$$

where we used (11), (13) and (15).

3.3 The multigrid shape optimization algorithm

At k-level of discretization, we consider a function $g_k : I \times \mathbb{R} \to \mathbb{R}$ to be defined iteratively in terms of g_{k+1}, where we set $g_K = 0$, being K the finest level of discretization. Let us introduce the following "perturbed" shape optimization problem

$$\min_{\Gamma_k \in \mathcal{U}_{ad}^k} F_k(\Gamma_k) := \hat{J}_k(\Gamma_k) - \int_{\Omega_k} g_k \, d\Omega , \tag{16}$$

where $\hat{J}_k$ represents the discrete reduced objective functional at k-level defined in (9). It is clear that at the finest level K, the problem (16) corresponds to the original discrete shape optimization problem. Our aim is to formulate a multigrid shape optimization scheme for solving the minimization problem (16) for all levels k. In the following we will work under the following natural regularity assumption on differentiability and local positivity of the shape Hessian. For a discussion on the shape Hessian see Section 6.

Assumption 3.1. *The functional $\hat{J}_k$ is twice shape differentiable and the shape Hessian is locally positive definite.*

Under the previous assumption, solving (16) is equivalent to solve the following gradient equation

$$\nabla \hat{J}_k(\Gamma_k) - g_{k|\Gamma_k} = 0 \quad \text{on } \Gamma_k , \tag{17}$$

where it is easy to show that $g_{k|\Gamma_k}$ is the shape gradient of the functional $\int_{\Omega_k} g_k d\Omega$, as the integrand does not depend on the domain Ω_k.

Next, we illustrate our multigrid optimization scheme. At level k, let a starting boundary Γ_k^0 be given. To solve (16), we apply m_1-steps of the one-grid GSO scheme as follows

$$\Gamma_k^{\ell+1} = G_k(\Gamma_k^\ell), \qquad \ell = 0, 1, \dots, m_1 - 1.$$

Now, denote with $\gamma_k \in \mathcal{U}_{ad}^k$ the shape-deformation error such that the solution Γ_k to (17) can be written as $\Gamma_k := \Gamma_k^{m_1} + \gamma_k \mathbf{e}_n$ and γ_k is solution to the following equation:

$$\nabla \hat{J}_k(\Gamma_k^{m_1} + \gamma_k \mathbf{e}_n) - g_{k|\Gamma_k} = 0 \quad \text{on } \Gamma_k := \Gamma_k^{m_1} + \gamma_k \mathbf{e}_n \, .$$

The above equation is equivalent to the following

$$\nabla \hat{J}_k(\Gamma_k^{m_1} + \gamma_k \mathbf{e}_n) - [\nabla \hat{J}_k(\Gamma_k^{m_1})]^\#_{|\Gamma_k^{m_1} + \gamma_k \mathbf{e}_n} = g_{k|\Gamma_k^{m_1} + \gamma_k \mathbf{e}_n} - [\nabla \hat{J}_k(\Gamma_k^{m_1})]^\#_{|\Gamma_k^{m_1} + \gamma_k \mathbf{e}_n} \, , \tag{18}$$

where we remark that $\nabla \hat{J}_k(\Gamma_k^{m_1} + \gamma_k \mathbf{e}_n)$ is defined on the boundary $\Gamma_k^{m_1} + \gamma_k \mathbf{e}_n$. Equation (18) is the starting point in order to construct a coarse-grid optimization problem. The general approach is to represent the operators and the functions on the left-hand side of (18) at the $(k-1)$-level, while the right-hand side is obtained by restriction. In particular, we define

$$\Gamma_{k-1} = I_k^{k-1} \Gamma_k^{m_1} + \gamma_{k-1} \mathbf{e}_n, \tag{19}$$

where $\gamma_{k-1} \in \mathcal{U}_{ad}^{k-1}$ denotes a coarse representation of the k-level shape-deformation error γ_k. Starting from (18), prolongating and restricting in a proper way, we define the following coarse-grid gradient problem on Γ_{k-1}

$$\nabla \hat{J}_{k-1}(\Gamma_{k-1}) - [\nabla \hat{J}_{k-1}(I_k^{k-1} \Gamma_k^{m_1})]^\#_{|\Gamma_{k-1}} = \mathcal{I}_k^{k-1} \left(g_{k|\Gamma_k^{m_1}} - [\nabla \hat{J}_k(\Gamma_k^{m_1})]^\#_{|\Gamma_k^{m_1}} \right). \tag{20}$$

We note that the shape gradient $\nabla \hat{J}_{k-1}(I_k^{k-1} \Gamma_k^{m_1})$ is defined on $I_k^{k-1} \Gamma_k^{m_1}$; hence it needs to be properly prolongated and restricted in order to be defined on Γ_{k-1}. The above equation for Γ_{k-1} can be written in the following form

$$\nabla \hat{J}_{k-1}(\Gamma_{k-1}) - g_{k-1|\Gamma_{k-1}} = 0, \tag{21}$$

where

$$g_{k-1} = \left[\mathcal{I}_k^{k-1} \left(g_{k|\Gamma_k^{m_1}} - [\nabla \hat{J}_k(\Gamma_k^{m_1})]^\#_{|\Gamma_k^{m_1}} \right) + \nabla \hat{J}_{k-1}(I_k^{k-1} \Gamma_k^{m_1}) \right]^\# .$$

Equivalently, by using the functional restriction operator defined in (13), we have

$$g_{k-1} = \left[I_k^{k-1} (g_{k|I} - [\nabla \hat{J}_k(\Gamma_k^{m_1})]^\#_{|I}) + \nabla \hat{J}_{k-1}(I_k^{k-1} \Gamma_k^{m_1}) \right]^\# . \tag{22}$$

Notice that the term

$$\tau_{k-1} = \nabla \hat{J}_{k-1}(I_k^{k-1} \Gamma_k^{m_1}) - \mathcal{I}_k^{k-1} \nabla \hat{J}_k(\Gamma_k^{m_1})$$

plays the role of a defect-correction term.

We are ready to introduce the "perturbed" shape optimization problem at $(k-1)$-level which reads as follows

$$\min_{\Gamma_{k-1} \in \mathcal{U}_{ad}^{k-1}} F_{k-1}(\Gamma_{k-1}) := \hat{J}_{k-1}(\Gamma_{k-1}) - \int_{\Omega_{k-1}} g_{k-1} \, d\Omega \, , \tag{23}$$

with $g_{k-1} : I \times \mathbb{R} \to \mathbb{R}$ defined as in (22). For clarity, it is convenient to collect some crucial properties of the coarse-grid optimization problem (21)-(22). The first result shows that, at convergence, all levels share the same solution which represents the fixed point of our multigrid scheme.

Proposition 3.1. *Suppose that $\Gamma_k^{m_1} = \Gamma_k$ solves the fine-grid gradient equation $\nabla \hat{J}_k(\Gamma_k) - g_{k|\Gamma_k} = 0$, then $\gamma_{k-1} = 0$.*

Proof. If $\Gamma_k^{m_1} = \Gamma_k$ solves the fine-grid gradient equation $\nabla \hat{J}_k(\Gamma_k) - g_{k|\Gamma_k} = 0$, then $\mathcal{I}_k^{k-1}(\nabla \hat{J}_k(\Gamma_k) - g_{k|\Gamma_k}) = 0$ and the coarse-grid gradient equation (20) becomes

$$\nabla \hat{J}_{k-1}(\Gamma_{k-1}) = [\nabla \hat{J}_{k-1}(I_k^{k-1}\Gamma_k)]^{\#}{}_{|\Gamma_{k-1}}$$

whose solution is $\Gamma_{k-1} = I_k^{k-1}\Gamma_k$. That is, the coarse-grid solution is the restriction of the fine-grid solution. Then, from (19) we obtain $\gamma_{k-1} = 0$. □

The second result compares the shape gradient of the functional F_k at any Γ_k with the shape gradient of F_{k-1} at $\Gamma_{k-1} = I_k^{k-1}\Gamma_k$.

Proposition 3.2. *The shape gradient of the coarse-grid functional F_{k-1} at $\Gamma_{k-1} = I_k^{k-1}\Gamma_k$ coincides with the restriction of the shape gradient of the fine-grid functional F_k at Γ_k.*

Proof. By using (22), we have the following result

$$\begin{aligned}
\nabla F_{k-1}(\Gamma_{k-1}) &= \nabla \hat{J}_{k-1}(\Gamma_{k-1}) - g_{k-1|\Gamma_{k-1}} \\
&= \nabla \hat{J}_{k-1}(\Gamma_{k-1}) - \Big[I_k^{k-1}(g_{k|I} - [\nabla \hat{J}_k(\Gamma_k)]^{\#}{}_{|I}) + \nabla \hat{J}_{k-1}(I_k^{k-1}\Gamma_k) \Big]^{\#}{}_{|\Gamma_{k-1}} \\
&= \Big[I_k^{k-1}([\nabla \hat{J}_k(\Gamma_k)]^{\#}{}_{|I} - g_{k|I}) \Big]^{\#}{}_{|\Gamma_{k-1}} \\
&= \mathcal{I}_k^{k-1} \nabla F_k(\Gamma_k), \qquad (24)
\end{aligned}$$

where in the last step we used (13). □

The key feature of our multigrid approach is to construct an effective descent direction using an approximate minimizer of the coarse-grid problem. To illustrate this fact, assume that $\tilde{\Gamma}_{k-1} \in \mathcal{U}_{ad}^{k-1}$ is an approximate minimizer on the coarse grid such that

$$F_{k-1}(\tilde{\Gamma}_{k-1}) < F_{k-1}(I_k^{k-1}\Gamma_k^{m_1}). \qquad (25)$$

We can obtain $\tilde{\Gamma}_{k-1}$ by using the one-grid GSO scheme or by recursive application of the present multigrid scheme. Therefore, using (19) yields an approximation to the shape-deformation error given by

$$\gamma_{k-1}\mathbf{e}_n = \tilde{\Gamma}_{k-1} - I_k^{k-1}\Gamma_k^{m_1}. \qquad (26)$$

Further, the prolongation of this function on the finer grid provides an approximation to the shape-deformation error γ_k at the k-level, as follows

$$\gamma_k = I_{k-1}^{k}\gamma_{k-1}. \qquad (27)$$

We next prove that $\gamma_k \mathbf{e}_n$, with γ_k given by (27), provides a descent direction for F_k at $\Gamma_k^{m_1}$. We remark that $\gamma_k \mathbf{e}_n$ needs to be prolongated to build a proper vector field $\gamma_k^{\#}\mathbf{e}_n$ defined in $I \times \mathbb{R}$ (see (14) for the definition of $\gamma^{\#}$).

Proposition 3.3. *There holds*

$$dF_k(\Gamma_k^{m_1}, {\gamma_k}^{\#}\mathbf{e}_n) = \int_{\Gamma_k^{m_1}} \nabla F_k(\Gamma_k^{m_1}) {\gamma_k}^{\#}\mathbf{e}_n \cdot \nu \, dS \; < 0 \,, \tag{28}$$

where ν is the outward normal vector to $\Omega_k^{m_1}$.

Proof. To prove (28), denote with $\hat{\Gamma}_{k-1} = I_k^{k-1}\Gamma_k^{m_1}$, then by using (25) we have

$$F_{k-1}(\tilde{\Gamma}_{k-1}) < F_{k-1}(\hat{\Gamma}_{k-1}). \tag{29}$$

Now, using local positiveness of the Shape Hessian $\nabla^2 F_{k-1}$ (see Assumption 3.1) and employing Taylor's expansion yield for any $\gamma \in \mathcal{U}_{ad}^{k-1}$

$$F_{k-1}(\hat{\Gamma}_{k-1} + \gamma \mathbf{e}_n) > F_{k-1}(\hat{\Gamma}_{k-1}) + \int_{\hat{\Gamma}_{k-1}} \nabla F_{k-1}(\hat{\Gamma}_{k-1}) \gamma^{\#}\mathbf{e}_n \cdot \nu \, dS \tag{30}$$

being ν the normal to $\hat{\Omega}_{k-1}$.

Let $\gamma = \gamma_{k-1}$ with γ_{k-1} given by (26), i.e., $\tilde{\Gamma}_{k-1} = \hat{\Gamma}_{k-1} + \gamma_{k-1}\mathbf{e}_n$, from (30) and (29) we obtain

$$0 > F_{k-1}(\hat{\Gamma}_{k-1} + \gamma_{k-1}\mathbf{e}_n) - F_{k-1}(\hat{\Gamma}_{k-1}) > \int_{\hat{\Gamma}_{k-1}} \nabla F_{k-1}(\hat{\Gamma}_{k-1}) \gamma_{k-1}^{\#} \, \mathbf{e}_n \cdot \nu \; dS \,. \tag{31}$$

Now we can prove (28). By using (27), (13) and (12) we have

$$\begin{aligned}
\int_{\Gamma_k^{m_1}} \nabla F_k(\Gamma_k^{m_1}) \gamma_k^{\#}\mathbf{e}_n \cdot \nu \, dS &= \int_{\Gamma_k^{m_1}} \nabla F_k(\Gamma_k^{m_1}) \mathcal{I}_{k-1}^k \gamma_{k-1}^{\#} \, \mathbf{e}_n \cdot \nu \, dS \\
&= \int_{I_k^{k-1}\Gamma_k^{m_1}} \mathcal{I}_k^{k-1} \nabla F_k(\Gamma_k^{m_1}) \gamma_{k-1}^{\#} \, \mathbf{e}_n \cdot \nu \, dS \\
&= \int_{I_k^{k-1}\Gamma_k^{m_1}} \nabla F_{k-1}(I_{k-1}^k \Gamma_k^{m_1}) \gamma_{k-1}^{\#} \, \mathbf{e}_n \cdot \nu \, dS < 0
\end{aligned}$$

where in the last step we used (24) and (31). □

Since $\gamma_k \mathbf{e}_n$, with γ_k given by (27), provides a descent direction, we define the coarse-to-fine minimization step as follows

$$\Gamma_k^{m_1+1} = \Gamma_k^{m_1} + \alpha \, \gamma_k \mathbf{e}_n,$$

where α is a steplength to be determined by a linesearch algorithm. Our multigrid optimization step is completed by applying m_2-steps of the one-grid GSO scheme as follows

$$\Gamma_k^{\ell+1} = G_k(\Gamma_k^{\ell}), \qquad \ell = m_1 + 1, \ldots, m_1 + m_2.$$

Summarizing, a minimizing sequence for the problem

$$\min F_k(\Gamma_k)$$

is obtained with the following multigrid optimization scheme.

Let Γ_k^0 be the initial optimization boundary at level k and g_k be given. The following steps define one multigrid V-cycle that will be denoted by $\Gamma_k^{new} = MGSO(\Gamma_k^{old}, k, g_k)$.

Algorithm 3.1 (Multigrid shape optimization (MGSO) scheme)**.**
If $k = 1$ (coarsest resolution) then the minimization problem (23) *is solved exactly. Else if $k > 1$:*

Step 1. Apply one-grid optimization

$$\Gamma_k^{\ell+1} = G_k(\Gamma_k^{\ell}), \qquad \ell = 0, 1, \ldots, m_1 - 1.$$

Step 2. Compute the gradient residual

$$r_k = g_{k|I} - [\nabla \hat{J}_k(\Gamma_k^{m_1})]^{\#}_{|I}.$$

Step 3. Restrict the residual and the approximate solution to coarse levels

$$r_{k-1} = I_k^{k-1} r_k, \qquad \hat{\Gamma}_{k-1} = I_k^{k-1} \Gamma_k^{m_1}.$$

Step 4. Setup the coarse-grid problem

$$g_{k-1} = [\nabla \hat{J}_{k-1}(\hat{\Gamma}_{k-1}) + r_{k-1}]^{\#}.$$

Step 5. Call the MGSO scheme to compute the coarse-grid minimizer for $\min F_{k-1}(\Gamma_{k-1})$*:* $\tilde{\Gamma}_{k-1} = MGSO(\hat{\Gamma}_{k-1}, k-1, g_{k-1})$ *such that*

$$\tilde{\Gamma}_{k-1} \approx \operatorname{argmin} F_{k-1}(\Gamma_{k-1}).$$

Step 6. Construct the multigrid coarse-to-fine descent direction

$$\gamma_k \mathbf{e}_n = I_{k-1}^k \left(\tilde{\Gamma}_{k-1} - \hat{\Gamma}_{k-1} \right).$$

Step 7. Optimize along γ_k with α-linesearch

$$\Gamma_k^{m_1+1} = \Gamma_k^{m_1} + \alpha\, \gamma_k \mathbf{e}_n$$

Step 8. Apply one-grid optimization

$$\Gamma_k^{\ell+1} = G_k(\Gamma_k^{\ell}), \qquad \ell = m_1 + 1, \ldots, m_1 + m_2.$$

Step 8. End.

It should be clear that the MGSO scheme given above will be applied iteratively, thus resulting in a sequence of V-cycles with finest level K and $g_K = 0$. Therefore, we also refer to the following algorithm as the MGSO scheme.

Algorithm 3.2 (MGSO Scheme)**.**
Input: Finest level K, initial Γ_K^0, $g_K = 0$, Tolerance ϵ, iteration counter $\ell = 0$, max number iterations ℓ_{max}.

Step 1. Compute $\Gamma_K^{\ell+1} = MGSO(\Gamma_K^{\ell}, K, g_K)$.

Step 2. Check convergence: if $\|\mathbb{S}(\nabla \hat{J}(\Gamma^\ell))\| > \epsilon$ *and* $\ell < \ell_{max}$ *go to Step 1.*

Step 3. End.

We remark that the MGSO scheme can be used as a standalone optimizer or it can be used as a preconditioner [34, 3] for another optimization scheme. Specifically, we notice that the use of different grids in the MGSO scheme result in better globalization properties that allow to start the MGSO scheme far away from the optimal solution. On the other hand, as in the multigrid scheme to solve PDE problems, the MGSO scheme should be applied to reach a solution error that is proportional to the truncation error of the problem being solved. Once this level of accuracy is reached, the computational cost of the MGSO scheme increases compared to the improvement obtained in the solution.

4 Numerical experiments

In this section, we aim at validating the numerical performance of our MGSO scheme defined by Algorithm 3.2. In the first example, we investigate the robustness of the MGSO algorithm and we compare it with a nonlinear conjugate gradient (NLCG) scheme. In particular, we consider different levels of discretization, different starting configurations and different choices of the optimization parameters. In the second example, we further test the numerical efficacy of the MGSO algorithm.

4.1 Example 1

In the first example, we consider the following model problem

$$\min_{(y,\Omega)} J(y,\Omega) := \frac{1}{2}\|y-\bar{y}\|^2_{0,\Omega} + \frac{\lambda}{2}(|\partial\Omega| - P)^2,$$

where y is the solution of the following Poisson problem

$$\begin{aligned} -\Delta y &= 20(x_1 - x_1^2 + x_2 - x_2^2) && \text{in } \Omega, \\ y &= 0 && \text{on } \partial\Omega, \end{aligned} \tag{32}$$

being $\bar{y}$ a given target function and $\lambda > 0$ a parameter penalizing the difference between the perimeter $|\partial\Omega|$ of Ω and a given target perimeter value P. We assume that the minimization is performed among the set of domains Ω with $\partial\Omega := \Gamma^F \cup \Gamma$, where $\Gamma^F := \{0\}\times(0,1)\cup(0,1)\times\{0\}\cup\{0\}\times(0,1)$ is fixed and Γ is the only part of the boundary that is free to move. We choose $\bar{y}(x_1,x_2) = 10(x_1 - x_1^2)(x_2 - x_2^2)$ and $P = 4$ such that the exact solution of the above minimization problem is given by $\Omega = (0,1)\times(0,1)$ and $y = \bar{y}$.

Throughout the section we have employed a stopping criterium based on the value of the normalized preconditioned gradient at the finest level of discretization. We have tested our MGSO scheme on a sequence of successively finer triangulations of two different initial domains and we have employed a stopping test based on the value of the normalized gradient at the finest level of discretization. We have considered two initial configurations: a first test case where an initial symmetric domain configuration is chosen (cf. Figure 2(a)), and a second test case with an initial unsymmetric domain configuration (cf. Figure 2(b)). We denote by h_0 the

corresponding coarsest initial mesh sizes (see Figure 3, left column). We have tested our MGSO scheme considering $K = 0, 1, 2, \ldots$ successive uniform refinements of these initial grids (see Figure 3, middle and right columns for $K = 1, 2$, respectively). In Figure 3, the degrees of freedom that are free to move are highlighted with black bullets. To approximate the solution of (32) we have employed piecewise linear

(a) Symmetric initial configuration: levels of refinement $K = 0, 1, 2$.

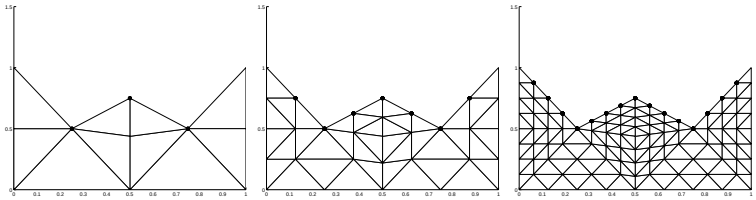

(b) Unsymmetric initial configuration: levels of refinement $K = 0, 1, 2$.

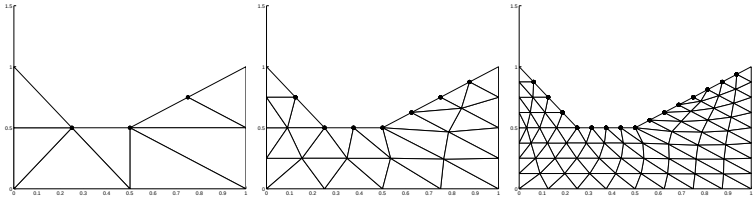

Figure 3: Initial domains and corresponding first two levels of refinement. The degrees of freedom that are free to move are highlighted with black bullets.

finite elements.

We have initially set $\lambda = 100$ and we have run our MGSO scheme with a relative tolerance for the normalized preconditoned residual set equal to 10^{-4}, employing $m_1 = m_2 = 2$ presmoothing and postsmoothing steps In Figure 4 we report some snapshots of the domains obtained by MGSO algorithm for K=1 and K=3 and the unsymmetric initial configuration shown in Figure 2(b). It is remarkable that after the first iteration the current geometry is already almost optimal (cf. Figures 3(a) (middle) and 3(b) (middle)) and the functional value has decreased in a substantial way (see Figure 6). Figure 6 also shows the quantity $\frac{1}{2}\|y - y_h\|^2_{0,\Omega}$ that measures the accuracy of the finite element approximation y_h on the current finest level of discretization. The analogous results obtained with the NLCG algorithm are collected in Figure 5. We note that, opposite to what observed for the MGSO scheme, the approximate domain obtained with one iteration of the NLCG algorithm is far from the optimal one (cf. Figure 5 (middle column) and the corresponding ones in Figure 4). Finally, we observe that the sequence of domains converges towards the optimal one slower than in the case of the MGSO scheme (see Figure 6 for a comparison between the corresponding histories of convergence). Concerning these results, our numerical experience is that the MGSO scheme defines an optimization direction that is superior to that obtained in the NLCG scheme. We remark that the computational cost of a MGSO V-cycle is larger than a NLCG step. However, the MGSO scheme is more efficient in the first phase of the optimization procedure. A similar result is obtained in [34] where a multigrid optimization scheme is used to solve variational problems.

(a) Finest level of discretization $K = 1$. Initial configuration (left), after 1 iteration (middle) and 12 iterations (right).

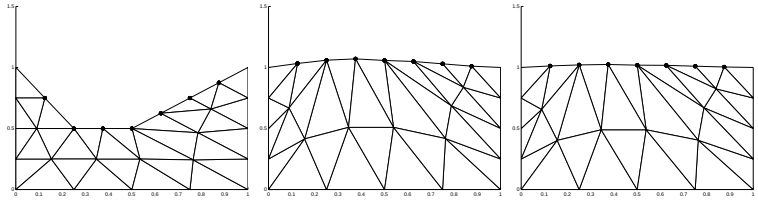

(b) Finest level of discretization $K = 3$. Initial configuration (left), after 1 iteration (middle) and 9 iterations (right).

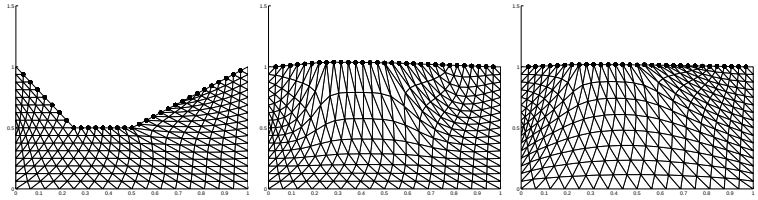

Figure 4: Performance of the MGSO scheme (see Algorithm 3.1) for different values of the finest level K of discretization. Unsymmetric initial configuration.

(a) Finest level of discretization $K = 1$. Initial configuration (left), after 1 iteration (middle) and 6 iterations (right).

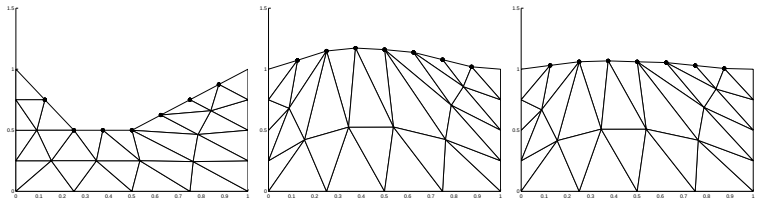

(b) Finest level of discretization $K = 3$. Initial configuration (left), after 1 iteration (middle) and 9 iterations (right).

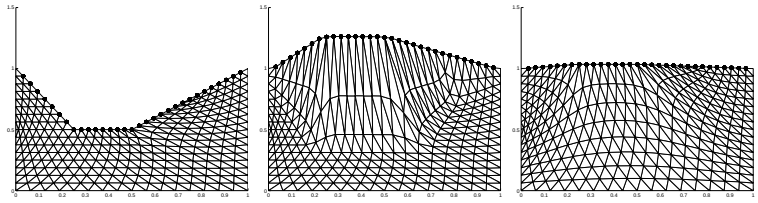

Figure 5: Performance of the NLCG scheme for different values of the finest level K of discretization. Unsymmetric initial configuration.

(a) History of convergence of functional value for different finest level of discretization: $K = 1$ (left) and $K = 3$ (right). The horizontal lines refer to the the quantity $\frac{1}{2}\|y - y_h\|^2_{0,\Omega}$, which measures the accuracy of the finite element approximation y_h on the current finest level of discretization.

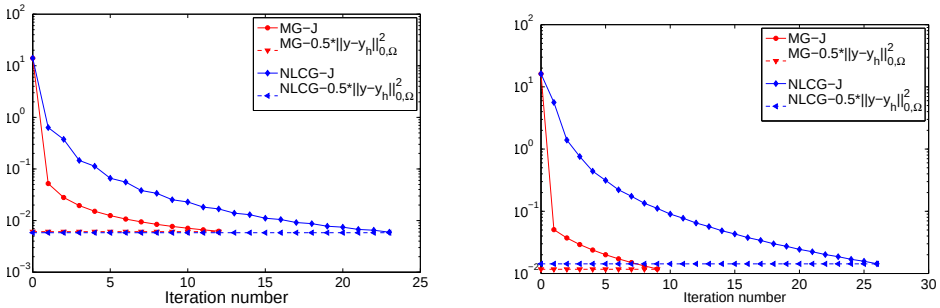

(b) History of convergence of normalized preconditioned residual for different finest level of discretization: $K = 1$ (left) and $K = 3$ (right). The horizontal lines refer to the stopping test tolerance.

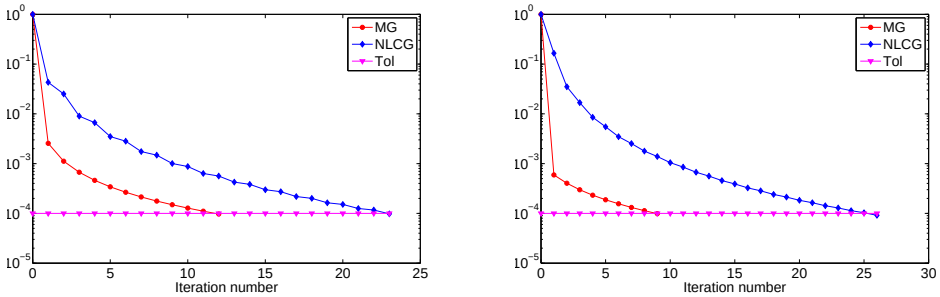

Figure 6: Histories of convergence of MGSO (circle) and NLCG (diamond) schemes: functional value (top) and normalized preconditioned residual (bottom). Unsymmetric initial configuration and different values of the finest level of discretization K are considered. The iteration number refers to a complete MGSO (or NLCG) iteration.

To test the robustness of our algorithm, we have run the MGSO scheme starting from a different initial configuration, namely a symmetric one (see Figure 7) and we have compared its performance with the one of the NLCG algorithm (see Figure 8). Finally, in Figure 9 we report the associated histories of convergence. As above, we note that our MGSO scheme is more effective in building descent directions for the cost functional, whose convergence towards the minimum value results to be remarkably fast.

(a) Finest level of discretization $K = 1$. Initial configuration (left), after 1 iteration (middle) and 3 iterations (right).

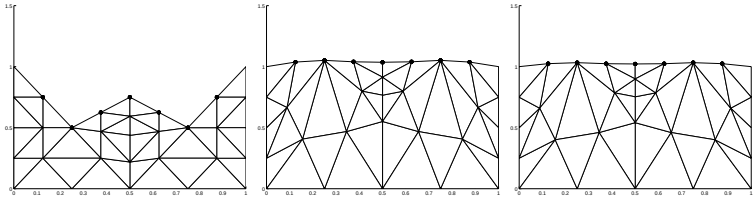

(b) Finest level of discretization $K = 3$. Initial configuration (left), after 1 iteration (middle) and 3 iterations (right).

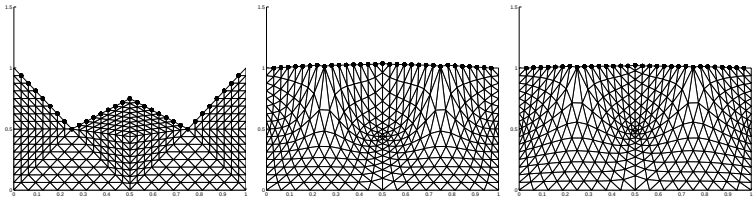

Figure 7: Performance of the MGSO scheme (see Algorithm 3.1) for different values of the finest level K of discretization. Symmetric initial configuration.

In Figure 10 (unsymmetric initial configuration) and in Figure 11 (symmetric initial configuration) we report the details of the grids and the directions obtained in Steps $1-8$ of MGSO scheme (see Algorithm 3.1) during the first iteration.
Finally, we have tested the robustness of our algorithm with respect to the value of the perimeter penalization parameter λ. We have run the MGSO scheme with $\lambda = 20$ and $\lambda = 50$ for unsymmetric and symmetric initial configurations and $K = 3$. In Figure 12 we report the histories of convergence (functional value, normalized preconditioned residual and the limiter $\frac{1}{2}\|y - y_h\|^2_{0,\Omega}$). We note, as expected, that the iteration counts needed for convergence increases as λ decreases (see Figures 6 and 9 for a comparison).

4.2 Example 2

Having already compared the efficiency of the MGSO scheme with the NLCG optimization algorithm, in this section we focus on the MGSO algorithm only. Let y be the solution of the following Poisson problem

$$\begin{aligned} -\Delta y &= -16\exp\left\{4(x_1-1/2)^2+4(x_2-1/2)^2\right\}(4x_1^2-4x_1+4x_2^2-4x_2+3) && \text{in } \Omega, \\ y &= 0 && \text{on } \partial\Omega. \end{aligned}$$

(a) Finest level of discretization $K = 1$. Initial configuration (left), after 1 iteration (middle) and 15 iterations (right).

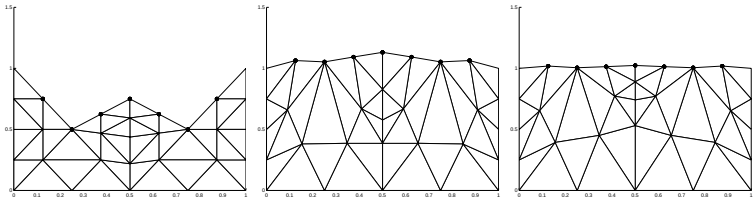

(b) Finest level of discretization $K = 3$. Initial configuration (left), after 1 iteration (middle) and 17 iterations (right).

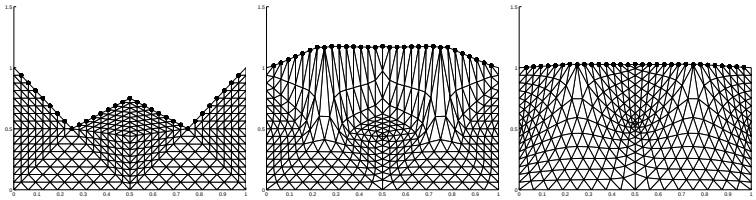

Figure 8: Performance of the NLCG scheme for different values of the finest level K of discretization. Symmetric initial configuration.

We consider the following model problem:

$$\min_{(y,\Omega)} J(y,\Omega) := \frac{1}{2}\,\|y-\bar{y}\|^2_{0,\Omega} + \frac{\lambda_P}{2}(|\partial\Omega| - P)^2 + \frac{\lambda_A}{2}(|\Omega| - A)^2,$$

where $\bar{y}$ is a target function, and $\lambda_P, \lambda_A > 0$ are parameters penalizing the difference between the perimeter $|\partial\Omega|$ of Ω and a given target perimeter value P, and the difference between the area $|\Omega|$ of Ω and a given target area value A, respectively. As before, we assume that the minimization is performed among the set of domains Ω with $\partial\Omega := \Gamma^F \cup \Gamma$, where $\Gamma^F := \{0\} \times (0,1) \cup (0,1) \times \{0\} \cup \{0\} \times (0,1)$ is fixed and Γ is the only part of the boundary that is free to move. We choose $\bar{y}(x_1,x_2) = \exp\left\{4(x_1-1/2)^2 + 4(x_2-/2)^2\right\} - \exp\{2\}$, $P = 3+\sqrt{2}\pi/4$ and $A = (\pi+6)/8$ such that the exact solution of the above minimization problem is given by

$$\Omega = \left\{(x_1,x_2) \in \mathbb{R}^2 \text{ s.t. } 0 < x_1 < 1 \text{ and } 0 < x_2 < 1/2 + \sqrt{1/2 - (x_1-1/2)^2}\right\}, \tag{33}$$

and $y = \bar{y}$ (cf. Figure 13). We have set $\lambda_A = 100$ and $\lambda_P = 10$, and we have run our MGSO scheme with two presmoothing and postsmoothing steps, and a relative tolerance for the normalized preconditoned residual set equal to 10^{-2}. Figure 14 shows the final mesh configurations obtained with the MGSO scheme; it can be seen that the optimal shape is clearly reached. Next, let $x_2^\Gamma(x_1) := 1/2 + \sqrt{1/2-(x_1-1/2)^2}$, $x_1 \in [0,1]$, i.e., $(x_1, x_2^\Gamma(x_1))$ defines the exact (curved) domain boundary Γ. We have measured the magnitude of the pointwise error $e_k = x_2^\Gamma(x_1^k) - x_2^k$, for any discretization point $P^k = (x_1^k, x_2^k)$ of the (polygonal) optimization boundary. Here P^k stands for the MGSO computed domain coordinate corresponding to the point x_k (at the final configuration). For different values of

(a) History of convergence of functional value for different finest level of discretization: $K = 1$ (left) and $K = 3$ (right). The horizontal lines refer to the the quantity $\frac{1}{2}\|y - y_h\|^2_{0,\Omega}$, which measures the accuracy of the finite element approximation y_h on the current finest level of discretization.

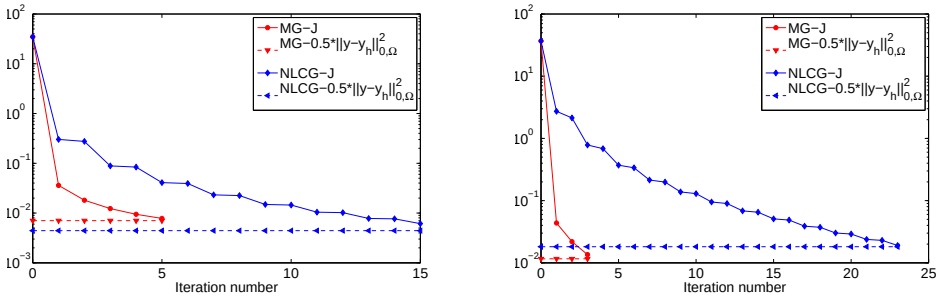

(b) History of convergence of normalized preconditioned residual for different finest level of discretization: $K = 1$ (left) and $K = 3$ (right). The horizontal lines refer to the stopping test tolerance.

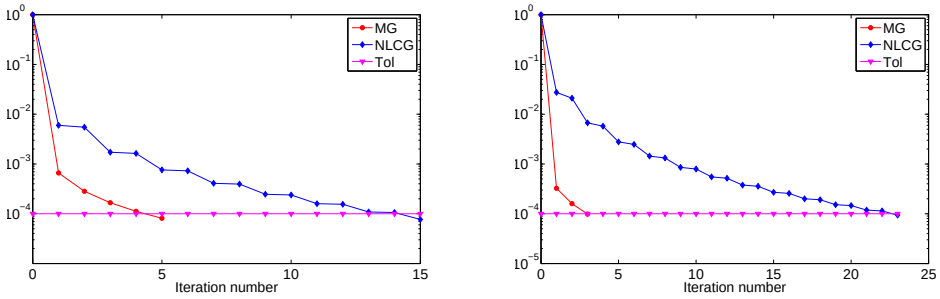

Figure 9: Histories of convergence of MGSO (circle) and NLCG (diamond) schemes: functional value (top) and normalized preconditioned residual (bottom). Symmetric initial configuration and different values of the finest level of discretization K are considered. The iteration number refers to a complete MGSO (or NLCG) iteration.

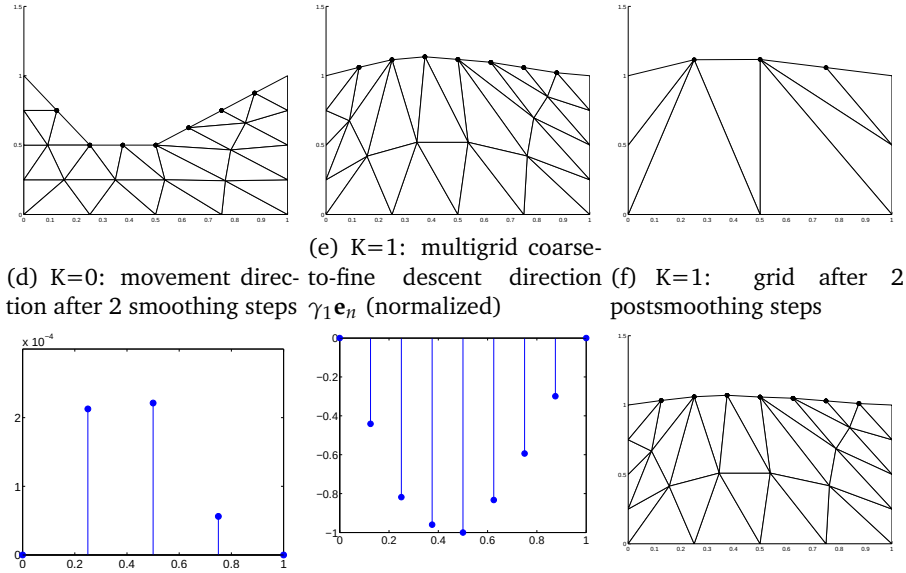

(a) K=1: initial grid

(b) K=1: grid after 2 presmoothing steps

(c) K=0: restricted grid

(d) K=0: movement direction after 2 smoothing steps

(e) K=1: multigrid coarse-to-fine descent direction $\gamma_1 \mathbf{e}_n$ (normalized)

(f) K=1: grid after 2 postsmoothing steps

Figure 10: Unsymmetric initial configuration and $K = 1$: grids and directions obtained in Steps $1 - 8$ of the MGSO scheme (iteration number 1).

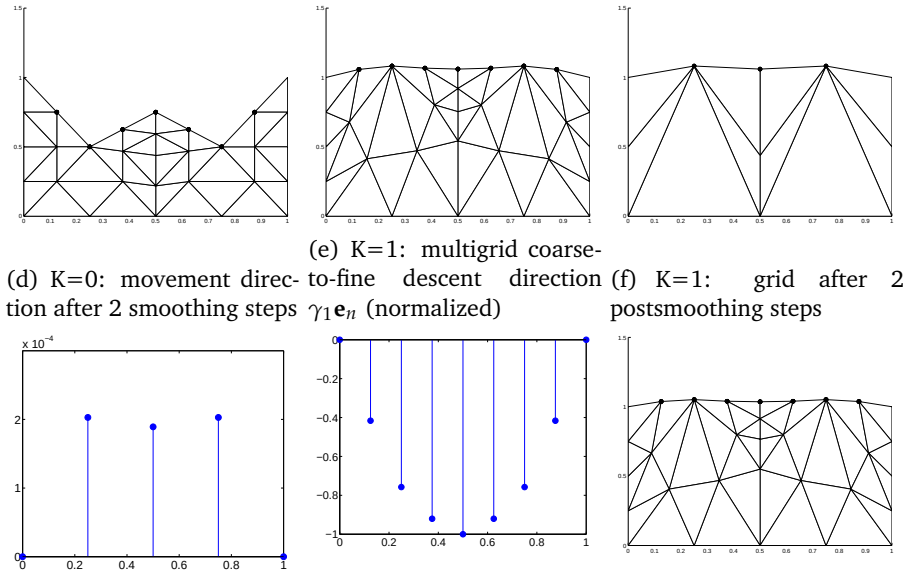

(a) K=1: initial grid

(b) K=1: grid after 2 presmoothing steps

(c) K=0: restricted grid

(d) K=0: movement direction after 2 smoothing steps

(e) K=1: multigrid coarse-to-fine descent direction $\gamma_1 \mathbf{e}_n$ (normalized)

(f) K=1: grid after 2 postsmoothing steps

Figure 11: Symmetric initial configuration and $K = 1$: grids and directions obtained in Steps $1 - 8$ of the MGSO scheme (iteration number 1).

(a) Unsymmetric initial configuration and $K = 3$

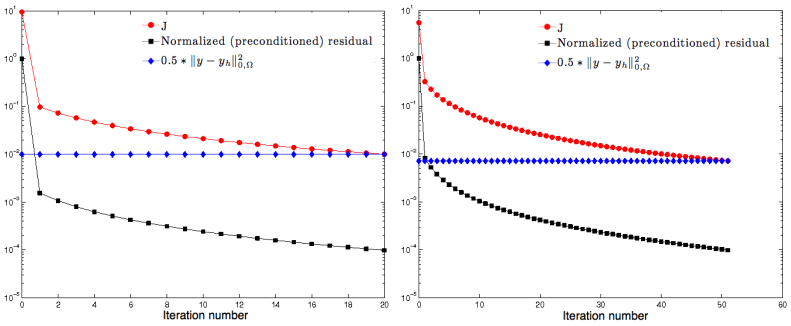

(b) Symmetric initial configuration and $K = 3$

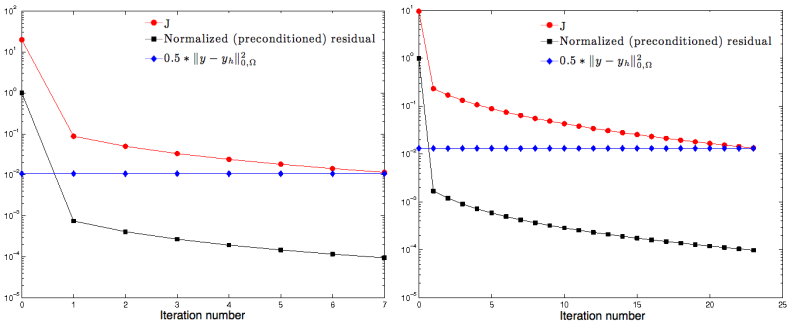

Figure 12: Histories of convergence of MGSO scheme for different values of the perimeter penalization parameter: $\lambda = 50$ (left) and $\lambda = 20$ (right). Functional values (circle) and normalized preconditioned residuals (square) are reported in the same plot together with the horizontal line indicating the level of accuracy of the finite element approximation. Unsymmetric (top) and symmetric (bottom) initial configurations and finest level of discretization $K = 3$ are considered.

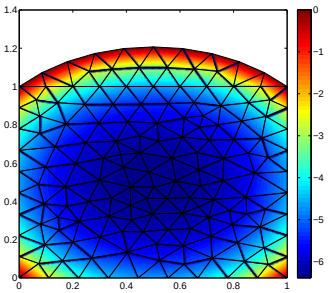

Figure 13: Exact solution of the minimization problem of Example 2.

(a) Initial mesh configurations for the discretization levels $K = 4, 5, 6$

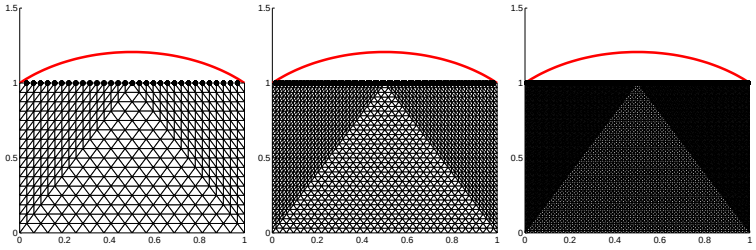

(b) Final mesh configurations of the MGSO scheme for the discretization levels $K = 4, 5, 6$

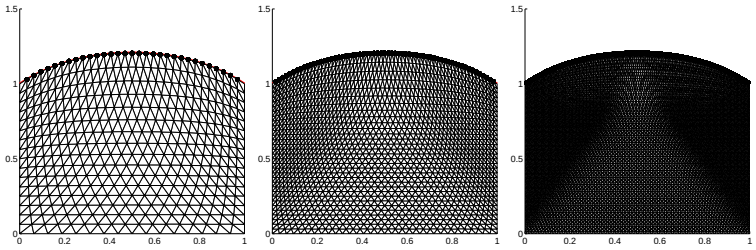

Figure 14: Initial (top) and final (bottom) mesh configurations of the MGSO scheme (see Algorithm 3.1) for different values of the finest level K of discretization (from left to right: $K = 4, 5, 6.$). The degrees of freedom that are free to move are highlighted with black bullets. The red line represents the boundary of the exact domain Ω, cf. (33).

the discretization level $K = 4, 5, 6$, the computed pointwise errors are shown in Figure 15. It can be seen that, as the mesh size goes to zero, the MGSO algorithm provides better and better approximations of Γ.

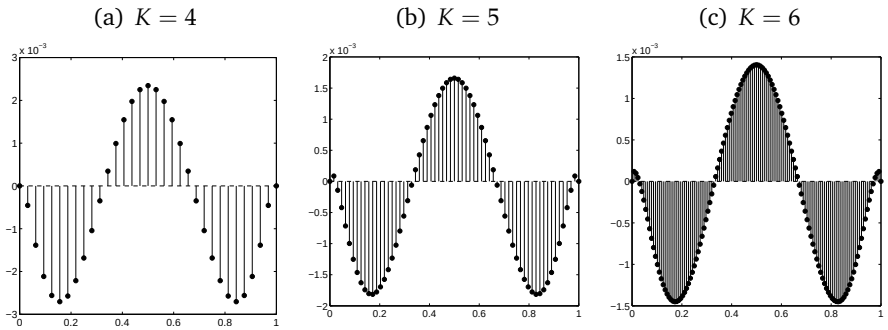

Figure 15: Pointwise error at the final MGSO configuration for different values of the discretization level $K = 4, 5, 6$.

5 Conclusion

A new multigrid shape optimization framework to solve elliptic PDE shape optimization problems was presented. This framework employs the Hadamard representation formula and defines the control boundary as the graph of a continuous function that can be approximated at various discretization levels. The multigrid shape optimization scheme was constructed based on

- the recursive application of geometrical intergrid transfer operators acting on the space of control boundaries;
- a coarse-grid correction resulting from the formulation of coarse shape optimization problems.

The convergence of the proposed multigrid shape optimization method was proved and validated through various numerical experiments that demonstrated the effectiveness of this methodology. Finally, it is useful to remark that the presented framework may be extended to treat possibly non-elliptic PDE shape optimization problems.

Acknowledgments

P.F.A. and M.V. were partially supported by Azione Integrata Italia-Spagna through the project IT097ABB10.

6 Appendix. Shape Hessian of a simple test problem

Let $y = y(\Omega)$ be the unique solution to the following elliptic partial differential equation

$$\begin{aligned} -\Delta y &= f \qquad \text{in } \Omega \qquad (34)\\ y &= y_b \qquad \text{on } \partial\Omega\,. \qquad (35)\end{aligned}$$

We consider the following cost functional depending on the solution y of the problem (34)-(35)

$$J(y,\Omega) := \frac{1}{2}\int_\Omega (y-\bar{y})^2\, d\Omega + \lambda \int_{\partial\Omega} dS,$$

with $\lambda > 0$.

We set $\hat{J}(\Gamma) = J(y(\Omega),\Omega)$. Let V be a given vector field and $\mathrm{v} = \langle V, \nu\rangle$. It is easy to check that the shape derivative of the functional $\hat{J}$ reads as follows

$$d\hat{J}(\Gamma)[V] := \int_\Gamma \left(\frac{1}{2}(y-\bar{y})^2 + \partial_\nu p\, \partial_\nu (y-y_b) + \lambda K\right) \mathrm{v}\, dS\,,$$

where K is the mean curvature, y is the solution to (34)-(35) and p is the solution to the following adjoint equation

$$\begin{aligned} -\Delta p &= y-\bar{y} \qquad \text{in } \Omega\\ p &= 0 \qquad \text{on } \Gamma.\end{aligned}$$

By following [5] the shape Hessian reads as follows

$$\begin{aligned} d^2\hat{J}(\Gamma)[V][W] &= \int_\Gamma \left(\partial_\nu p'[W]\, \partial_\nu (y-y_b) + \partial_\nu p\, \partial_\nu y'[W]\right) \mathrm{v}\, dS + \lambda \int_\Gamma \nabla_\Gamma \mathrm{v} \nabla_\Gamma \mathrm{w}\, dS\\ &\quad + \int_\Gamma \nabla\cdot\left[\left(\frac{1}{2}(y-\bar{y})^2 + \partial_\nu p\, \partial_\nu (y-y_b)\right) V\, dS\right] \mathrm{w}\,.\end{aligned}$$

where $p'[W]$ solves

$$\begin{aligned} -\Delta p'[W] &= y'[W] \qquad \text{in } \Omega\\ p'[W] &= -\partial_\nu p\, W\cdot\nu \qquad \text{on } \partial\Omega\,.\end{aligned}$$

If we assume that Γ is such that $d\hat{J}(\Gamma)[V] = 0$ for all V, then the shape Hessian reduces to

$$d^2\hat{J}(\Gamma)[V][W] = \int_\Gamma \left(\partial_\nu p'[W]\, \partial_\nu (y-y_b) + \partial_\nu p\, \partial_\nu y'[W]\right) \mathrm{v}\, dS + \lambda \int_\Gamma \nabla_\Gamma \mathrm{v} \nabla_\Gamma \mathrm{w}\, dS\,. \qquad (36)$$

In view of the study of the positive definiteness of the shape Hessian of $\widehat{J}$, we focus on the first term on the right-hand side of (36), as the contribution of the second term is clear. In doing this, we closely follow [27] and we analyze the

symbol of the shape Hessian of the functional $\hat{J} = \frac{1}{2}\int_\Omega (y-\bar{y})^2\, d\Omega$, where y solves (34)-(35). Let us recall that

$$d\hat{J}(\Gamma)[V] := \int_\Gamma G\, \mathrm{v}\, dS \quad \text{with } G = \frac{1}{2}(y-\bar{y})^2 + \partial_\nu p\, \partial_\nu (y-y_b)\,. \tag{37}$$

Let $\varphi(s)$ be a parametrization of Γ, i.e., $\Gamma = \{\varphi(s) :\ s \in [0,L]\}$. Given a function $\alpha(s)$, we consider a domain deformation of the type $\Gamma^\varepsilon(\alpha) = \{\varphi(s) + \varepsilon\alpha(s)\nu(s) :\ s \in [0,L]\}$. The shape Hessian of $\hat{J}(\Gamma)$ in direction $W = \alpha\nu$ is the limit

$$d^2\hat{J}(\Gamma)[V][W] = \lim_{\varepsilon\to 0} \frac{d\hat{J}(\Gamma^\varepsilon)[V] - d\hat{J}(\Gamma)[V]}{\varepsilon}\,.$$

In the following we denote by $\widetilde{G}[\alpha]$ the perturbation of the shape gradient G when the vector filed $W = \alpha\nu$ is applied to the boundary Γ. By using (37), we get

$$\widetilde{G}[\alpha] = (y-\bar{y})y'[\alpha] + \partial_\nu p'[\alpha]\, \partial_\nu (y-y_b) + \partial_\nu p\, \partial_\nu y'[\alpha]$$

where the shape derivatives $p'[\alpha] := p'[W]$ and $y'[\alpha] := y'[W]$ solve respectively

$$\begin{aligned} -\Delta p'[\alpha] &= y'[\alpha] \ \text{ in } \Omega, \qquad & p'[\alpha] &= -\partial_\nu p\, \alpha \ \text{ on } \Gamma,\\ -\Delta y'[\alpha] &= 0 \ \text{ in } \Omega, \qquad & y'[\alpha] &= -\partial_\nu (y-y_b)\, \alpha \ \text{ on } \Gamma. \end{aligned}$$

In the following, we assume that $\Omega = \{(x_1,x_2) :\ x_1 \in \mathbb{R}, x_2 > 0\}$ is the upper-half plane, which means that the normal to the boundary $\Gamma = \{(x_1,0) :\ x \in \mathbb{R}\}$ is directed as the x_2-axis and the perturbed gradient reads as follows

$$\widetilde{G}[\alpha] = (y-\bar{y})y'[\alpha] + \partial_{x_2} p'[\alpha]\, \partial_{x_2} (y-y_b) + \partial_{x_2} p\, \partial_{x_2} y'[\alpha]\,.$$

We set $\alpha = e^{i\omega_1 x_1}$ and we also assume that the output perturbations of the primal and adjoint variables are of the form

$$\begin{aligned} y'[\alpha] &= \widehat{y} e^{i\omega_1 x_1} e^{\omega_2 x_2}\\ p'[\alpha] &= \widehat{p} e^{i\omega_1 x_1} e^{\omega_2 x_2}. \end{aligned}$$

Due to the boundary conditions of the perturbed states $y'[\alpha]$ and $p'[\alpha]$ we have that

$$\widehat{y} = -\partial_{x_2}(y-y_b) \qquad \widehat{p} = -\partial_{x_2} p\,. \tag{38}$$

Now we perform a local analysis of the Hessian. The coefficients $\widehat{y}$ and $\widehat{p}$ satisfy the linear system

$$\begin{pmatrix} -(-\omega_1^2+\omega_2^2) & 0 \\ -1 & -(-\omega_1^2+\omega_2^2) \end{pmatrix} \begin{pmatrix} \widehat{y} \\ \widehat{p} \end{pmatrix} = \begin{pmatrix} 0 \\ 0 \end{pmatrix} \tag{39}$$

which can be thought as Laplace problems for y' and p' in the Fourier space. The two equations (38) and (39) are non-contradicting, if the above matrix has not full rank, i.e., if

$$\omega_1 = |\omega_2|\,.$$

Thus we have

$$\partial_{x_2} y'[\alpha]_{|x_2=0} = -(\partial^2_{x_2x_2}(y-y_b) + \partial_{x_2}(y-y_b)|\omega_1|)\alpha$$
$$\partial_{x_2} p'[\alpha]_{|x_2=0} = -(\partial^2_{x_2x_2} p + \partial_{x_2} p|\omega_1|)\alpha$$

with $\alpha = e^{i\omega_1 x_1}$. Hence,

$$\widetilde{G}[\alpha] = -\Big[(y-\bar{y})\partial_{x_2}(y-y_b) + \partial_{x_2}(y-y_b)(\partial^2_{x_2x_2} p + \partial_{x_2} p|\omega_1|) + \partial_{x_2} p(\partial^2_{x_2x_2}(y-y_b) + \partial_{x_2}(y-y_b)|\omega_1|)\Big]\,\alpha\,.$$

This means that the shape Hessian is a pseudo-differential operator of order one.

References

[1] A. BONITO AND J. E. PASCIAK, *Convergence analysis of variational and non-variational multigrid algorithms for the Laplace-Beltrami operator*, accepted for publication on Mathematics of Computation.

[2] A. BORZÌ, *On the convergence of the MG/OPT method*, PAMM, 5 (1) (2005), pp. 735–736.

[3] A. BORZÌ AND V. SCHULZ, *Computational Optimization of Systems Governed by Partial Differential Equations*, SIAM, 2011.

[4] D. BEGIS AND R. GLOWINSKI, *Application de la méthode des éléments finis à l'approximation d'un problème de domaine optimal. Méthodes de résolution des problèmes approchś* Appl. Math. Optim. 2 (2) (1975/76), pp. 130–169.

[5] D. BUCUR AND J.P. ZOLÉSIO, *Anatomy of the shape Hessian via Lie Brackets*, Annali di Matematica pura e applicata, 173 (1) (1997), pp. 127–143.

[6] F. BEUX AND A. DERVIEUX, *A hierarchical approach for shape optimization*, Engrg. Comput. 11 (1) (1994), pp. 25–48.

[7] M. BURGER, *A framework for the construction of level set methods for shape optimization and reconstruction*, Interfaces Free Bound. 5 (2003) 301-329.

[8] J.-A. DÉSIDÉRI, B.A. EL MAJD AND A. JANKA, *Nested and self-adaptive Bézier parameterizations for shape optimization*, J. Comput. Phys., 224 (1) (2007), pp. 117–131.

[9] J.-A. DÉSIDÉRI, *Hierarchical optimum-shape algorithms using embedded Bezier parameterizations*. In: Y. Kuznetsov et al., Editors, Numerical Methods for Scientific Computing, Variational Problems and Applications, CIMNE, Barcelona (2003).

[10] J.-A. DÉSIDÉRI AND A. JANKA, *Multilevel shape parameterization for aerodynamic optimization ? application to drag and noise reduction of transonic/supersonic business jet*, in: E. Heikkola et al., (Ed.), European Congress on Computational Methods in Applied Sciences and Engineering (ECCOMAS 2004).

[11] J.-A. DÉSIDÉRI, *Two-level ideal algorithm for parametric shape optimization*, in: W. Fitzgibbon, R. Hoppe, J. Periaux, O. Pironneau, Y. Vassilevski (Eds.), Advances in Numerical Mathematics, Proceedings of International Conferences, Moscow (2005).

[12] J.-A. DÉSIDÉRI AND A. DERVIEUX, *Hierarchical methods for shape optimization in aerodynamics - I: multilevel algorithms for parametric shape optimization*, in: J. Periaux and H. Deconinck, (Eds.), Introduction to Optimization and Multidisciplinary Design, Lecture Series 2006-3, Von Karman Institute for Fluid Dynamics Publish., 2006.

[13] F. DE GOURNAY, *Velocity extension for the level-set method and multiple eigenvalues in shape optimization*, SIAM J. Control Optim. 45 (2006) 343-367.

[14] M.C. DELFOUR AND J.-P. ZOLESIO, Shapes and geometries analysis, differential calculus, and optimization, SIAM, 2011.

[15] G. DOGAN, P. MORIN, R.H. NOCHETTO AND M. VERANI, *Discrete gradient flows for shape optimization and applications*, Comput. Methods Appl. Mech. Engrg. 196 (2007) 3898-3914.

[16] K. EPPLER, S. SCHMIDT, V. SCHULZ, AND C. ILIC, *Preconditioning the pressure tracking in fluid dynamics by shape Hessian information*, Journal of Optimization Theory and Applications, 141 (3) (2009), pp. 513-531.

[17] M.D. GUNZBURGER, H. KIM, AND S. MANSERVISI, *On a shape control problem for the stationary Navier-Stokes equations*, M2AN, 34 (2000), pp. 1233–1258.

[18] R. KORNHUBER; H. YSERENTANT, *Multigrid methods for discrete elliptic problems on triangular surfaces*, Comput. Vis. Sci. 11 (4) (2008), 251–257.

[19] M. LAUMEN, *Newton's method for a class of optimal shape design problems*, SIAM J. Optim., 10 (2) (2003), pp. 503-533.

[20] R. M. LEWIS AND S. G. NASH, *Model problems for the multigrid optimization of systems governed by differential equations*, SIAM Journal on Scientific Computing, 26 (6) (2005), pp. 1811–1837.

[21] J.L. LIONS, *Optimal control of systems governed by partial differential equations*, Springer, Berlin, 1971.

[22] B. MOHAMMADI AND O. PIRONNEAU, *Applied Shape Optimization for Fluids*, Oxford University Press, 2001.

[23] P. MORIN, R.H. NOCHETTO, S. PAULETTI AND M. VERANI, *Adaptive finite element method for shape optimization*, accepted for publication on ESAIM: Control, Optimisation and Calculus of Variations.

[24] S. G. NASH, *A multigrid approach to discretized optimization problems*, Optimization Methods and Software, 14 (1 & 2) (2000), pp. 99–116.

[25] J. NOCEDAL, AND S.J. WRIGHT, Numerical optimization, Springer-Verlag, New York, 1999.

[26] O. PIRONNEAU, Optimal shape design for elliptic systems, Springer, 1984.

[27] S. SCHMIDT, V. SCHULZ, *Impulse Response Approximations of Discrete Shape Hessians with Application in CFD*, SIAM Journal on Control and Optimization, 48(4) (2009), pp. 2562–2580.

[28] J. SOKOLOWSKI AND J.-P. ZOLESIO, *Introduction to Shape Optimization*, Shape Sensitivity Analysis, Springer Verlag, Berlin, 1992.

[29] S. TA'ASAN, *Introduction to Shape Design and Control, Inverse Design and Optimisation Methods*, von Karman Institute Lecture Notes, VKI LS 1997-05.

[30] S. TA'ASAN AND G. KURUVILA AND M.D. SALAS, *Aerodynamic design and optimization in one shot*, 30th Aerospace Sciences Meeting, Reno, NV, AIAA Paper 92-0025, 1992.

[31] U. TROTTENBERG, C. OOSTERLEE, AND A. SCHÜLLER, *Multigrid*, Academic Press, London, 2001.

[32] M. VALLEJOS AND A. BORZÌ, *Multigrid optimization methods for linear and bilinear elliptic optimal control problems*, Computing, 82 (2008), 31-52.

[33] J.C. VASSBERG, AND A. JAMESON, *Aerodynamic Shape Optimization*, Part I & II, Von Karman Institute, Brussels, Belgium, 2006.

[34] Z. WEN AND D. GOLDFARB, *Line search multigrid methods for large-scale nonconvex optimization*, SIAM Journal on Optimization, 20 (2009), pp. 1478-1503

MOX Technical Reports, last issues

Dipartimento di Matematica "F. Brioschi",
Politecnico di Milano, Via Bonardi 9 - 20133 Milano (Italy)

47/2011 Antonietti, P.F.; Borz, A.; Verani, M.
Multigrid shape optimization governed by elliptic PDEs

46/2011 Migliorati, G.; Nobile, F.; von Schwerin, E.; Tempone, R.
Analysis of the discrete L2 projection on polynomial spaces with random evaluations

45/2011 Canuto, C.; Nochetto, R. H.; Verani, M.
Adaptive Fourier-Galerkin Methods

44/2011 Fumagalli,A.; Scotti,A.
Numerical modelling of multiphase subsurface flow in the presence of fractures

43/2011 L. Formaggia, A. Quarteroni, C. Vergara
On the physical consistency of the coupling between three-dimensional compliant and one-dimensional problems in haemodynamics

42/2011 Antonietti, P.F.; Quarteroni, A.
Numerical performance of discontinuous and stabilized continuous Galerkin methods or convection-diffusion problems

41/2011 Burman, E.; Zunino, P.;
Numerical Approximation of Large Contrast Problems with the Unfitted Nitsche Method

40/2011 D Angelo, C.; Zunino, P.; Porpora, A.; Morlacchi, S.; Migliavacca, F.
Model reduction strategies enable computational analysis of controlled drug release from cardiovascular stents

39/2011 Antonietti, P.F.; Ayuso de Dios, B.; Brenner, S.C.; Sung, L.-Y.
Schwarz methods for a preconditioned WOPSIP method for elliptic problems

38/2011 Porpora A., Zunino P., Vergara C., Piccinelli M.
Numerical treatment of boundary conditions to replace lateral branches in haemodynamics